[19] Wohl, J. G. "Maintainability prediction revisited: Diagnostic behavior, system complexity, and repair time," *IEEE Trans. Syst. Man Cybern.*, vol. SMC-12, no. 3, May/June 1982.
[20] Wohl, J. G. "Cognitive capability versus system complexity in electronic maintenance," *IEEE Trans. Syst. Man Cybern.*, vol. SMC-13, no. 4, July/Aug. 1983.

Moment-Preserving Curve Detection

LING-HWEI CHEN AND WEN-HSIANG TSAI, MEMBER, IEEE

Abstract — **A novel method for curve detection based on the moment-preserving principle is proposed. The method can be used to estimate curve locations and widths to subpixel accuracy. For each 4.5-unit circle in an input image that includes a curve segment, the approach derives a parabolic equation as well as a width value to describe the curve segment. Experimental results are included to show the effectiveness of the proposed detector.**

I. Introduction

Curve detection plays an important role in image processing. Several main steps in image processing, such as image encoding, compression, segmentation, and object recognition, depend on successful extraction of curvilinear features. There are also many applications, such as mapping, drafting, and cartooning, that require robust algorithms for extracting curvilinear features from images.

Several curve detectors have been developed [1]. Rosenfeld and Thurston [2], [3] presented a nonlinear matched filtering curve detector. Arbitrary smooth curves are detected by the use of various local line detection operators in which different masks are used to determine curve directions and widths. The method cannot be used to detect corners and curves that are not smooth. Wu and Rosenfeld [4] proposed the use of the x and the y projections of an image to locate corners in the image. Paler *et al.* [5] also presented a method for detecting corner points in a scene, based on features extracted from the distribution of ordered gray-level values within a local window.

All these algorithms detect curves only to the "pixel" level, and most of them do not detect curve widths. Some problems, such as calibration, remotely sensed imagery curve detection, image-to-image and image-to-map registration, etc., need accurate measurement. A few algorithms have been developed to meet the need. The Hough transform is a method for detecting curves to subpixel accuracy. The approach involves applying a coordinate transformation to the picture such that all the points belonging to a curve C of a given type map into a single location P in the transformed space. The coordinates of P are just the coefficients of the equation describing C. Based on the curve equation, the curve locations can be calculated to subpixel accuracy [6]–[8]. Ballard [9] presented a generalized Hough transform to detect arbitrary shapes. All these methods assume that the curve points have been known and use these curve points to extract the parameter of the curve. Therefore, their effectiveness depends on the successful extraction of curve points.

Based on the moment-preserving principle which has been used in several other applications [10]–[13], Chen and Tsai [14] proposed a line detector that can be used to estimate line locations and widths to subpixel accuracy. The method can also be used to detect smooth curves. Based on the assumption that the curve points are nearly straight locally, the approach derives a line equation to approximate the curve points in a detection area. It is inapplicable when the curve points are not nearly linear locally or when a corner exists in the detection area. In short, each of the aforementioned methods, except the Hough transform, can detect either smooth curves or corners but not both. In this correspondence, a unified method is proposed that can be used for detecting all types of curvilinear features, including smooth curves, lines, corners, and unsmooth curves. The proposed approach assumes that the background on either side of the detected curve is the same. Based on the moment-preserving principle, the approach derives a parabolic equation as well as a width value to estimate the curve location and width locally to subpixel accuracy.

In the remainder of this correspondence, we first describe the proposed curve detector. The parabolic equation is then derived and the equation coefficients solved. Finally, some experimental results are presented to show the effectiveness of the proposed method and its superiority to conventional line-type curve detectors in curved feature and corner detection.

Manuscript received December 3, 1986; revised August 15, 1987.
The authors are with the Department of Information Science, National Chiao Tung University, Hsinchu, Taiwan 30050, Republic of China.
IEEE Log Number 8718863.

II. Proposed Curve Detector

The proposed curve detector approximates a curve segment with any thickness by a parabolic segment represented by its *central parabola* (i.e., the skeleton of the "thicker" parabola) and *width* (i.e., the curve "thickness"). Similar to [10], the proposed detector accepts as input the gray values of a set of 69 pixels arranged in such a way to best approximate the area of a circle with 4.5 units in radius:

		255	0	0	0	255		
	255	255	0	0	0	255	255	
255	255	255	0	0	0	255	255	255
0	0	0	0	0	0	255	255	255
0	0	0	0	0	0	255	255	255
0	0	0	0	0	0	255	255	255
255	255	255	255	255	255	255	255	255
	255	255	255	255	255	255	255	
		255	255	255	255	255.		

The detector generates as output a central parabolic equation, a parabolic width, and two intensity values h_1 and h_2 (assume $h_2 > h_1$). The detector separates the circle into two regions A_1 (curve area) and A_2 (background) with h_1 and h_2 as the representative intensity values for A_1 and A_2, respectively, as illustrated in Fig. 1.

In the sequel, the central parabola will be denoted as P, and the symmetrical axis of P will be denoted as SP. In this approach, we assume that SP passes through the center of the circle and that its direction is defined to be toward P (see Fig. 2(a)). This is reasonable because the circle size is small. Note that if SP does not pass through the center of the circle, a certain technique has been proposed to solve the problem, which will be discussed later in Section V. If the angle between SP and the positive X axis is q, we can rotate the circle counterclockwise with respect to the origin through an angle of $\pi/2 - q$ so that the rotated SP coincides with the Y axis (see Fig. 2(b)). Then the new coordinates (x', y') of any rotated point can be expressed by the coordinates (x, y) of the corresponding original unrotated point as

$$x' = x \sin q - y \cos q$$
$$y' = x \cos q + y \sin q, \tag{1}$$

and the equation for the rotated P can be expressed as

$$y' = ax'^2 + b. \tag{2}$$

0018-9472/88/0100-0148$01.00 ©1988 IEEE

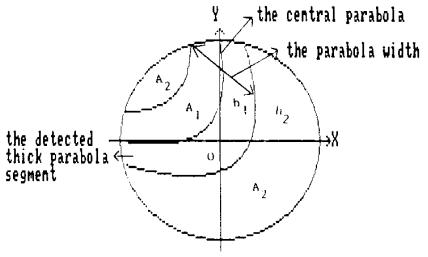

Fig. 1. Curve detection on 4.5-unit circle. Output data with $h_1 = 0$, $h_2 = 255$.

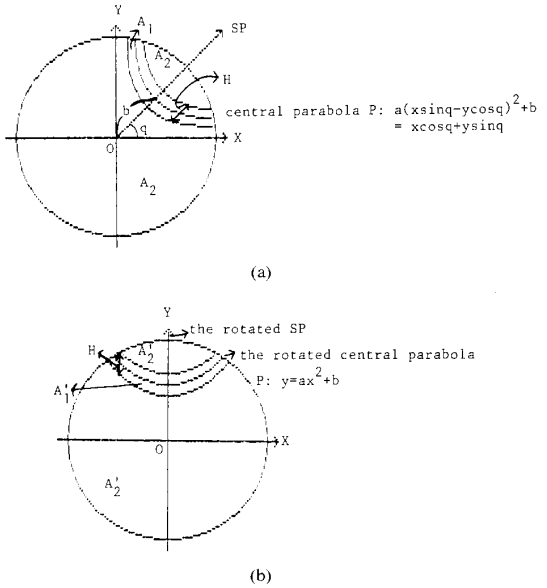

Fig. 2. Parabola before and after rotation. (a) Parabolic pattern expressed by its width H and its central parabolic equation as function of a, b, q. (b) Central parabolic equation as function of a, b only, after parabola is rotated counterclockwise with respect to origin through angle of $\pi/2 - q$.

Let H be the parabolic width that is measured in the direction as SP (see Fig. 2); then the two boundary parabolas of the rotated parabolic segment can be expressed as

$$y' = ax'^2 + b + H/2 \tag{3}$$

$$y' = ax'^2 + b - H/2. \tag{4}$$

Combining (1)–(4), we get the original central parabolic equation as

$$a(x\sin q - y\cos q)^2 + b = x\cos q + y\sin q \tag{5}$$

and the two boundary parabolas of the original parabolic segment as

$$a(x\sin q - y\cos q)^2 + b + H/2 = x\cos q + y\sin q$$

$$a(x\sin q - y\cos q)^2 + b - H/2 = x\cos q + y\sin q.$$

Therefore, the four parameters q, a, b, and H uniquely determine the detected parabolic segment. In the next two sections two analytic equations for computing q will first be derived, followed by three other nonlinear equations for calculating a, b, and H.

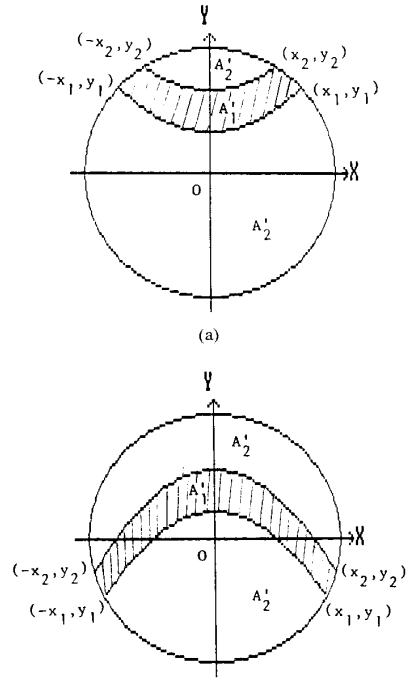

Fig. 3. Two rotated boundary parabolas intersect circle at four points (x_1, y_1), $(-x_1, y_1)$, (x_2, y_2), $(-x_2, y_2)$. (a) $x_1 \geq x_2$. (b) $x_1 < x_2$.

III. Derivations of the Equations for Computing the q Parameter

In this section several theorems will be proved from which two analytic equations for computing the q parameter can be derived. Recall that the curve detector is applied to a 4.5-unit circle, resulting in a central parabolic equation described by (5) and a width H, and that the circle is separated into two regions A_1 (parabola) and A_2 (background) with intensity values h_1 and h_2, respectively. First, we define

$$\bar{x} = \frac{h_1 \iint_{A_1} x\,dx\,dy + h_2 \iint_{A_2} x\,dx\,dy}{h_1 \iint_{A_1} dx\,dy + h_2 \iint_{A_2} dx\,dy} \tag{6}$$

$$\bar{y} = \frac{h_1 \iint_{A_1} y\,dx\,dy + h_2 \iint_{A_2} y\,dx\,dy}{h_1 \iint_{A_1} dx\,dy + h_2 \iint_{A_2} dx\,dy} \tag{7}$$

as the coordinates of the center of gravity of the intensities of the output data inside the circle [10].

If we rotate the 4.5-unit circle counterclockwise with respect to the origin through an angle of $\pi/2 - q$ (see Fig. 2), then the rotated SP will coincide with the Y axis. Let $(\bar{x}', \bar{y}')$ be the coordinates of the center of gravity of the intensities inside the rotated circle, in which there are two different regions A_1', A_2' (see Fig. 2(b)). Then $(\bar{x}', \bar{y}')$ are related to $(\bar{x}, \bar{y})$ through (1) [15].

Let BP_1, BP_2 be the two boundary parabolas of the rotated parabolic pattern (with width H). Assume that BP_1 and BP_2 intersect the circle at four points (x_1, y_1), $(-x_1, y_1)$, (x_2, y_2), and $(-x_2, y_2)$. Two cases can be identified here. One is $x_1 \geq x_2$ (see Fig. 3(a)); the other is $x_1 < x_2$ (see Fig. 3(b)). For each case, different equations will be developed.

Theorem 1: If $x_1 \geq x_2$ and the rotated parabolic segment intersects the 4.5-unit circle in any one of the eight distinct ways shown in Fig. 4, then $\bar{x}' = 0$ and $\bar{y}' < 0$.

Proof: Since both A_1' and A_2' are symmetric to themselves about the Y axis, it is easily seen that $\bar{x}' = 0$. To show that $\bar{y}' < 0$ for the cases shown in Fig. 4, let us redraw Fig. 4 as shown in Fig. 5. In Fig. 5 each circle is divided into several subregions B, D, C_d, and/or C_b. A_1' is composed of B and C_b, and A_2' of D and C_d. It follows that

$$\bar{y}' = \frac{h_1 \iint_{A_1'} y'\,dx'\,dy' + h_2 \iint_{A_2'} y'\,dx'\,dy'}{h_1 \iint_{A_1'} dx'\,dy' + h_2 \iint_{A_2'} dx'\,dy'}$$

$$= \frac{h_1\left(\iint_{B} y'\,dx'\,dy' + \iint_{C_b} y'\,dx'\,dy'\right)}{h_1 \iint_{A_1'} dx'\,dy' + h_2 \iint_{A_2'} dx'\,dy'}$$

$$+ \frac{h_2\left(\iint_{D} y'\,dx'\,dy' + \iint_{C_d} y'\,dx'\,dy'\right)}{h_1 \iint_{A_1'} dx'\,dy' + h_2 \iint_{A_2'} dx'\,dy'}. \tag{8}$$

Since C_d and C_b both are symmetric to themselves about the X axis, the integration value over C_d or C_b in the previous equation is zero. Therefore, (8) can be simplified to be

$$\bar{y}' = \frac{h_1 \iint_{B} y'\,dx'\,dy' + h_2 \iint_{D} y'\,dx'\,dy'}{h_1 \iint_{A_1'} dx'\,dy' + h_2 \iint_{A_2'} dx'\,dy'},$$

which can be further reduced to be

$$\bar{y}' = \frac{(h_1 - h_2) \iint_{B} y'\,dx'\,dy'}{h_1 \iint_{A_1'} dx'\,dy' + h_2 \iint_{A_2'} dx'\,dy'} \tag{9}$$

because B is symmetric to D about the X axis. Since $h_2 > h_1$ and the area of B is not zero, we get $\bar{y}' < 0$ and the theorem is proved.

By Theorem 1 and the fact that $(\bar{x}', \bar{y}')$ are the rotated version of $(\bar{x}, \bar{y})$, we immediately have the following theorem.

Theorem 2: If $x_1 \geq x_2$ and the rotated parabolic segment intersects the 4.5-unit circle in any one of the eight distinct ways shown in Fig. 4, then the direction of the vector from the origin to $(-\bar{x}, -\bar{y})$ is identical to the direction of SP, i.e., $(-\bar{x}, -\bar{y})$ is on SP.

By Theorem 2, we have the following corollary whose proof is easy and is omitted.

Corollary: If $x_1 \geq x_2$ and the rotated parabolic segment intersects the 4.5-unit circle in any one of the eight distinct ways shown in Fig. 4, then the angle q between SP and the positive X-axis satisfies the equations

$$\cos q = \frac{-\bar{x}}{\sqrt{\bar{x}^2 + \bar{y}^2}} \tag{10}$$

$$\sin q = \frac{-\bar{y}}{\sqrt{\bar{x}^2 + \bar{y}^2}}. \tag{11}$$

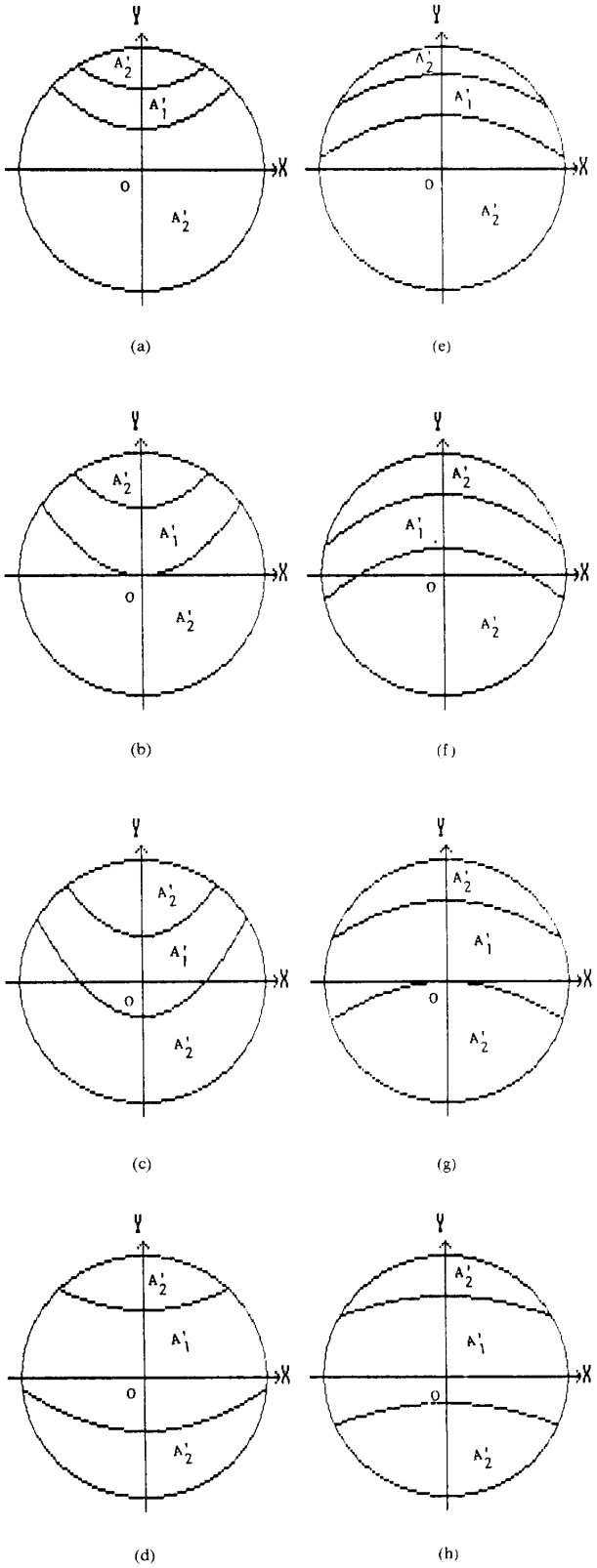

Fig. 4. Eight possible cases (not exhaustive) in which rotated parabolic segment might intersect 4.5-unit circle when $x_1 \geq x_2$.

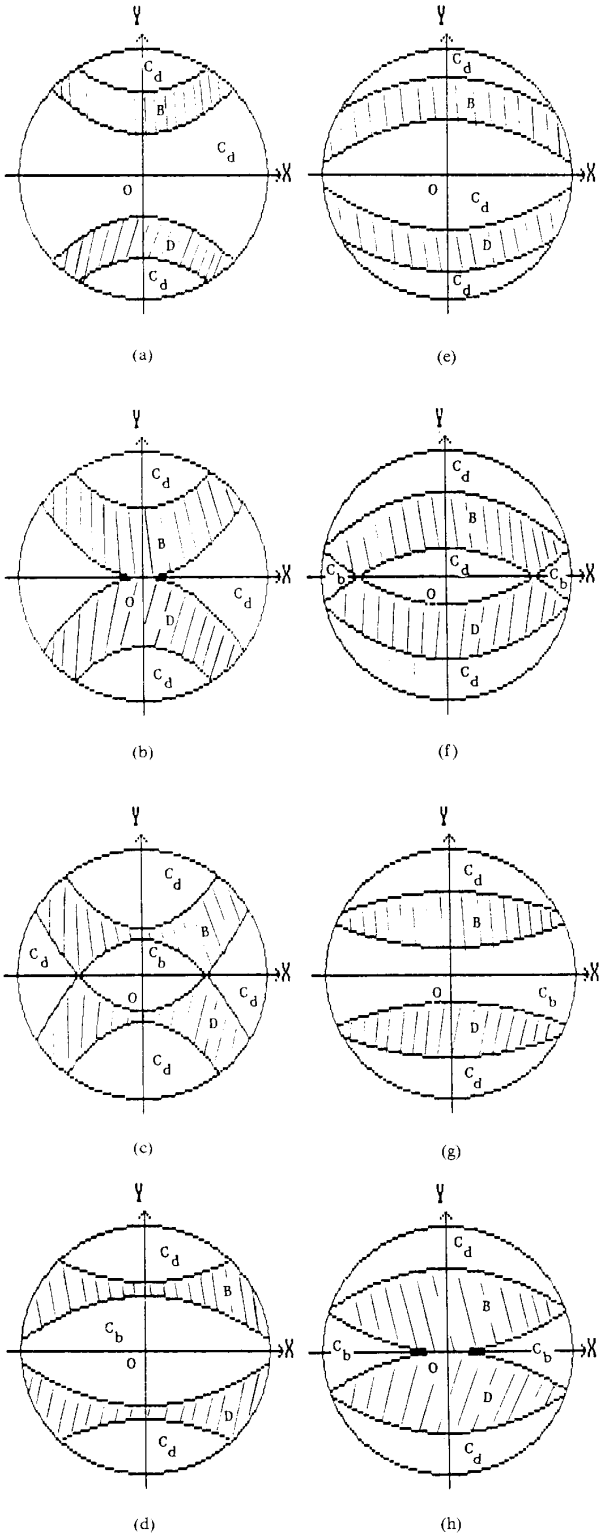

Fig. 5. Circle in each case of Fig. 4 is divided to consist of several types of subregions B, D, C_d, and/or C_b. C_b and C_d both are symmetric to themselves about X axis. B is symmetric to D about X axis. (a) $A_1' = B$, $A_2' = D \cup C_d$. (b) $A_1' = B$, $A_2' = D \cup C_d$. (c) $A_1' = B \cup C_b$, $A_2' = D \cup C_d$. (d) $A_1' = B \cup C_b$, $A_2' = D \cup C_d$. (e) $A_1' = B$, $A_2' = D \cup C_d$. (f) $A_1' = B \cup C_b$, $A_2' = D \cup C_d$. (g) $A_1' = B \cup C_b$, $A_2' = D \cup C_d$. (h) $A_1' = B \cup C_b$, $A_2' = D \cup C_d$.

Let the grids of the 4.5-unit circle be indexed as

		1	2	3	4	5		
	12	11	10	9	8	7	6	
13	14	15	16	17	18	19	10	21
30	29	28	27	26	25	24	23	22
31	32	33	34	35	36	37	38	39
48	47	46	45	44	43	42	41	40
49	50	51	52	53	54	55	56	57
	64	63	62	61	60	59	58	
		65	66	67	68	69.		

Then $(\bar{x}, \bar{y})$ used in (10) and (11) can be approximated from input data as follows [14]:

$$\bar{x} = \frac{\sum_{j=1}^{k} x_j I_j W_j}{\sum_{j=1}^{k} I_j W_j} \tag{12}$$

$$\bar{y} = \frac{\sum_{j=1}^{k} y_j I_j W_j}{\sum_{j=1}^{k} I_j W_j}, \tag{13}$$

where

I_j	intensity associated with the jth grid,
W_j	weight associated with the jth grid,
(x_j, y_j)	coordinates of the center of the jth grid,
k	69.

Here we take W_j to be the fraction of the intersection area of the jth grid and the disk enclosed by the 4.5-unit circle. This leads to the following W_j values:

$$W_j = \begin{cases} 0.0084670539, & j = 1,5,13,21,49,57,65,69; \\ 0.0137929169, & j = 2,4,22,30,40,48,66,68; \\ 0.013068037, & j = 6,12,58,64; \\ 0.01557318963, & j = 3,31,39,67; \\ 0.015719006, & \text{otherwise.} \end{cases}$$

Now for those cases shown in Fig. 4, we have completed the derivation of (10) and (11) for calculating the q parameter. For the other cases (including $x_1 < x_2$), we can get $\bar{x}_1' = 0$ similarly. However, it is hard to decide whether $\bar{y}' > 0$ or $\bar{y}' < 0$ in advance. For this, we can assume $\bar{y}' < 0$ and estimate q as before. If the detection result is unsatisfactory, then we can reverse the assumption (i.e., assume $\bar{y}' > 0$), and evaluate q by the following two equations:

$$\cos q = \frac{\bar{x}}{\sqrt{\bar{x}^2 + \bar{y}^2}} \tag{14}$$

$$\sin q = \frac{\bar{y}}{\sqrt{\bar{x}^2 + \bar{y}^2}}. \tag{15}$$

IV. Derivations of the Equations for Computing Parameters a, b, H

First, define the first three sample moments of the empirically obtained data in the 4.5-unit circle C as

$$m_i = \sum_{j=1}^{69} W_j I_j^i, \qquad i = 1,2,3.$$

By preserving the first three moments in the output of the

detector, we get the following three equalities:

$$P_1 h_1 + P_2 h_2 = m_1$$
$$P_1 h_1^2 + P_2 h_2^2 = m_2$$
$$P_1 h_1^3 + P_2 h_2^3 = m_3,$$

where the three left terms of the equations are the first three moments of the output data in the disk C, and the fractions P_1 and P_2 are

$$P_1 = a_1/(4.5^2\pi)$$
$$P_2 = 1 - P_1 = a_2/(4.5^2\pi).$$

Note that a_1 and a_2 are the areas of A_1 and A_2, respectively. Now, the foregoing equations can be solved to obtain P_1, P_2, h_1, and h_2 as follows [11]:

$$h_1 = (1/2)\left[-c_1 - \left(c_1^2 - 4c_0\right)^{1/2}\right]$$
$$h_2 = (1/2)\left[-c_1 - \left(c_1^2 - 4c_0\right)^{1/2}\right]$$
$$P_1 = (1/P_d)\begin{vmatrix} 1 & 1 \\ m_1 & h_2 \end{vmatrix}$$
$$P_2 = 1 - P_1$$

where

$$P_d = \begin{vmatrix} 1 & 1 \\ h_1 & h_2 \end{vmatrix}$$
$$c_0 = (1/c_d)\begin{vmatrix} -m_2 & m_1 \\ -m_3 & m_2 \end{vmatrix}$$
$$c_1 = (1/c_d)\begin{vmatrix} 1 & -m_2 \\ m_1 & -m_3 \end{vmatrix}$$
$$c_d = m_2 - m_1^2.$$

After knowing P_1 and P_2, a_1 and a_2 can be computed by

$$a_1 = P_1\pi(4.5)^2 \qquad a_2 = P_2\pi(4.5)^2.$$

These two values will be used in (16), (21), (21′), (27), and (27′) derived later.

Rotating the 4.5-unit circle counterclockwise with respect to the origin through an angle of $\pi/2 - q$, we can get the rotated parabolic segment as shown in Fig. 4 for some cases of $x_1 \geq x_2$. In the following, we only investigate Fig. 4(a); the other cases (including those for $x_1 < x_2$) can be treated similarly. Geometric relations existing in the detection circle area will be used to derive three simultaneous equations expressed in terms of a, b, and H. The equations will then be solved by numerical analysis techniques to obtain the values for a, b, and H.

Theorem 3: The following equality is true:

$$x_1 y_1 - x_2 y_2 - 2a\left(x_1^3 - x_2^3\right)/3 - 2b(x_1 - x_2) + H(x_1 + x_2) + R^2\left[\cos^{-1}(y_1/R) - \cos^{-1}(y_2/R)\right] = a_1 \tag{16}$$

where (x_1, y_1) and (x_2, y_2) satisfy the following equations:

$$x_1^2 + y_1^2 = R^2 \tag{17}$$
$$ax_1^2 + (b - H/2) = y_1 \tag{18}$$
$$x_2^2 + y_2^2 = R^2 \tag{19}$$
$$ax_2^2 + (b + H/2) = y_2 \tag{20}$$
$$R = 4.5.$$

Proof: From Fig. 6, we see that the shaded area a_1 of the parabolic pattern can be computed as

$$a_1 = \iint_{A_1'} dy\,dx = \iint_{A_{11}} dy\,dx + \iint_{A_{12}} dy\,dx + \iint_{A_{13}} dy\,dx$$
$$= x_1 y_1 - x_2 y_2 - 2a\left(x_1^3 - x_2^3\right)/3 - 2b(x_1 - x_2) + H(x_1 + x_2) + R^2(\theta_1 - \theta_2).$$

Since $\theta_1 = \cos^{-1}(y_1/R)$, $\theta_2 = \cos^{-1}(y_2/R)$, we can get (16) easily, and the theorem is proved.

Theorem 4: The following equalities are true:

$$r^2 = \Big[(h_2 - h_1)\Big(a^2/5\left(x_2^5 - x_1^5\right) + (1 + 2a(b - H/2))/3\left(x_2^3 - x_1^3\right) + 2bHx_2 + \left(R^2 - (b - H/2)^2\right)(x_1 - x_2) + 2aHx_2^3/3\Big)/(h_1 a_1 + h_2 a_2)\Big]^2 \quad \text{for } x_1 \geq x_2 \tag{21}$$

$$r^2 = \Big[(h_2 - h_1)\Big(a^2/5\left(x_1^5 - x_2^5\right) + (1 + 2a(b + H/2))/3\left(x_1^3 - x_2^3\right) + \left(R^2 - (b + H/2)^2\right)(x_1 - x_2) + 2aHx_1^3/3 + 2bHx_1\Big)/(h_1 a_1 + h_2 a_2)\Big]^2 \quad \text{for } x_1 < x_2 \tag{21′}$$

where $r = \sqrt{\bar{x}^2 + \bar{y}^2}$ is the distance from the origin to the original center of gravity.

Proof: Since

$$r^2 = \bar{x}^2 + \bar{y}^2 = \bar{x}'^2 + \bar{y}'^2 = \bar{y}'^2, \tag{22}$$

substituting (8) into (22),

$$r^2 = \frac{\left(h_1 \iint_{A_1'} y'\,dx'\,dy' + h_2 \iint_{A_2'} y'\,dy'\,dx'\right)^2}{(h_1 a_1 + h_2 a_2)^2}$$
$$= \frac{\left(h_2 \iint_{C} y'\,dx'\,dy' - h_2 \iint_{A_1'} y'\,dy'\,dx' + h_1 \iint_{A_1'} y'\,dx'\,dy'\right)^2}{(h_1 a_1 + h_2 a_2)^2}$$
$$= \frac{\left[(h_1 - h_2) \iint_{A_1'} y'\,dx'\,dy'\right]^2}{(h_1 a_1 + h_2 a_2)^2}$$
$$= \Big[(h_2 - h_1)\Big(a^2/5\left(x_2^5 - x_1^5\right) + (1 + 2a(b - H/2))/3\left(x_2^3 - x_1^3\right) + 2bHx_2 + \left(R^2 - (b - H/2)^2\right)(x_1 - x_2) + 2aHx_2^3/3\Big)\Big]^2 / (h_1 a_1 + h_2 a_2)^2.$$

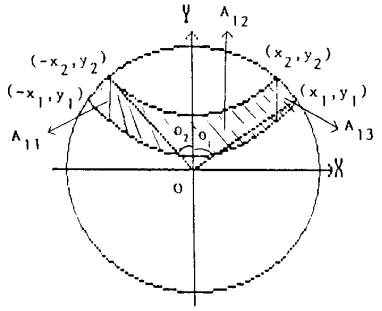

Fig. 6. Two rotated boundary parabolas intersect the circle at four points (x_1, y_1), $(-x_1, y_1)$, (x_2, y_2), $(-x_2, y_2)$, with $x_1 \geq x_2$, and the shaded region $A_1' = A_{11} \cup A_{12} \cup A_{13}$

Similarly, for $x_1 < x_2$, we can get (21'), and the theorem is proved.

Similarly to defining $\bar{x}$ and $\bar{y}$ ((6) and (7)), we can define

$$\overline{x^2} = \frac{h_1 \iint_{A_1} x^2\,dx\,dy + h_2 \iint_{A_2} x^2\,dx\,dy}{h_1 \iint_{A_1} dx\,dy + h_2 \iint_{A_2} dx\,dy} \tag{23}$$

$$\overline{xy} = \frac{h_1 \iint_{A_1} xy\,dx\,dy + h_2 \iint_{A_2} xy\,dx\,dy}{h_1 \iint_{A_1} dx\,dy + h_2 \iint_{A_2} dx\,dy} \tag{24}$$

$$\overline{y^2} = \frac{h_1 \iint_{A_1} y^2\,dx\,dy + h_2 \iint_{A_2} y^2\,dx\,dy}{h_1 \iint_{A_1} dx\,dy + h_2 \iint_{A_2} dx\,dy} \tag{25}$$

$$\overline{x'^2} = \frac{h_1 \iint_{A_1'} x'^2\,dx'\,dy' + h_2 \iint_{A_2'} x'^2\,dx'\,dy'}{h_1 \iint_{A_1'} dx'\,dy' + h_2 \iint_{A_2'} dx'\,dy'} \tag{26}$$

where x' and y' are the coordinates of the rotated circle. Then we have the following theorem.

Theorem 5: The following equalities are true:

$$\begin{aligned}&\big[(h_2-h_1)\big(R^4/4(\theta_1-\theta_2+\sin 4\theta_2/4-\sin 4\theta_1/4)\\&\quad+2a/5\big(x_1^5-x_2^5\big)\\&\quad+2(b-H/2)/3\big(x_1^3-x_2^3\big)-2Hx_2^3/3\big)\\&\quad+\pi R^4h_2/4\big]/(h_1a_1+h_2a_2)\\&\quad=\overline{x^2}\sin^2 q-2\overline{xy}\sin q\cos q+\overline{y^2}\cos^2 q,\qquad \text{for } x_1\geq x_2\end{aligned} \tag{27}$$

$$\begin{aligned}&\big[(h_2-h_1)\big(R^4/4(\theta_2-\theta_1-\sin 4\theta_2/4+\sin 4\theta_1/4)\\&\quad+2a/5\big(x_1^5-x_2^5\big)\\&\quad+2(b-H/2)/3\big(x_1^3-x_2^3\big)-2Hx_2^3/3\big)\\&\quad+\pi R^4h_2/4\big]/(h_1a_1+h_2a_2)\\&\quad=\overline{x^2}\sin^2 q-2\overline{xy}\sin q\cos q+\overline{y^2}\cos^2 q,\qquad \text{for } x_1< x_2\end{aligned} \tag{27'}$$

where

$$\theta_1 = \cos^{-1}(x_1/R),$$
$$\theta_2 = \cos^{-1}(x_2/R).$$

Proof: By (26) we have

$$\overline{x'^2} = \frac{h_1 \iint_{A_1'} x'^2\,dx'\,dy' + h_2 \iint_{A_2'} x'^2\,dx'\,dy'}{h_1 \iint_{A_1'} dx'\,dy' + h_2 \iint_{A_2'} dx'\,dy'}.$$

For $x_1 \geq x_2$, the foregoing can be further decomposed, according to Fig. 6, to be

$$\begin{aligned}\overline{x'^2} &= \Big[h_2 \iint_C x'^2\,dx'\,dy'\\&\quad+(h_1-h_2)\iint_{A_1'} x'^2\,dx'\,dy'\Big]\Big/(h_1a_1+h_2a_2)\\&=\Big[h_2\iint_C x'^2\,dx'\,dy'+(h_1-h_2)\\&\quad\cdot\Big(\iint_{A_{11}} x'^2\,dx'\,dy'+\iint_{A_{12}} x'^2\,dx'\,dy'\\&\quad+\iint_{A_{13}} x'^2\,dx'\,dy'\Big)\Big]\Big/(h_1a_1+h_2a_2)\\&=\big[(h_2-h_1)\big(R^4/4(\theta_1-\theta_2+\sin 4\theta_2/4-\sin 4\theta_1/4)\\&\quad+2a/5\big(x_1^5-x_2^5\big)+2(b-H/2)/3\big(x_1^3-x_2^3\big)-2Hx_2^3/3\big)\\&\quad+\pi R^4h_2/4\big]/(h_1a_1+h_2a_2).\end{aligned} \tag{28}$$

On another hand, combining (1) and (23)–(26), we have

$$\begin{aligned}\overline{x'^2} &= \frac{h_1 \iint_{A_1'} x'^2\,dx'\,dy' + h_2 \iint_{A_2'} x'^2\,dx'\,dy'}{h_1 \iint_{A_1'} dx'\,dy' + h_2 \iint_{A_2'} dx'\,dy'}\\&=\Big[h_1\iint_{A_1}(x\sin q-y\cos q)^2\,dx\,dy\\&\quad+h_2\iint_{A_2}(x\sin q-y\cos q)^2\,dx\,dy\Big]\Big/\\&\quad\Big(h_1\iint_{A_1}dx\,dy+h_2\iint_{A_2}dx\,dy\Big)\\&=\Big[\sin^2 q\Big(h_1\iint_{A_1}x^2\,dx\,dy+h_2\iint_{A_2}x^2\,dx\,dy\Big)\\&\quad-2\sin q\cos q\Big(h_1\iint_{A_1}xy\,dx\,dy+h_2\iint_{A_2}xy\,dx\,dy\Big)\\&\quad+\cos^2 q\Big(h_1\iint_{A_1}x^2\,dx\,dy+h_2\iint_{A_2}x^2\,dx\,dy\Big)\Big]\Big/(h_1a_1+h_2a_2)\\&=\overline{x^2}\sin^2 q-2\overline{xy}\sin q\cos q+\overline{y^2}\cos^2 q.\end{aligned} \tag{29}$$

Combining (29) and (28), we can get (27) for $x_1 \geq x_2$. Similarly, we can get (27') for $x_1 < x_2$, and the theorem is proved.

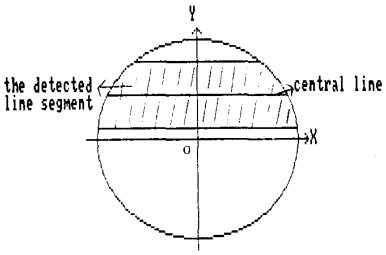

Fig. 7. Result of applying proposed detector to line pattern is same as that of applying Chen–Tsai line detector. —central line equation $y = 2$.

Here, $\overline{x^2}$, $\overline{xy}$, and $\overline{y^2}$ used in (27) and (27′) can be approximated from input data as follows:

$$\overline{x^2} = \frac{\sum_j I_j \iint_{G_j \cap C} x^2\,dx\,dy}{\sum_j I_j \iint_{G_j \cap C} dx\,dy} \tag{30}$$

$$\overline{xy} = \frac{\sum_j I_j \iint_{G_j \cap C} xy\,dx\,dy}{\sum_j I_j \iint_{G_j \cap C} dx\,dy} \tag{31}$$

$$\overline{y^2} = \frac{\sum_j I_j \iint_{G_j \cap C} y^2\,dx\,dy}{\sum_j I_j \iint_{G_j \cap C} dx\,dy}, \tag{32}$$

where G_j is the area of the jth grid, and C is the area of the 4.5-unit detection circle. Now, solving x_1, y_1, x_2, and y_2 appearing in (16), (21), (21′), (27), and (27′), we can get x_1, y_1, x_2, and y_2 in terms of a, b, and H by (17)–(20). Therefore, (16), (21), and (27) become three nonlinear equations with three unknown parameters a, b, and H for $x_1 \geqslant x_2$, and (16), (21′), and (27′) become three nonlinear equations with three unknown parameters a, b, and H for $x_1 < x_2$. A numerical method must be used to get the solutions. For this, the Newton's method [16] is used.

For the method to result in accurate solutions, we must start with good initial values (a_0, b_0, H_0) that are near the desired solutions. In general, most curves in an image are approximately linear locally. Therefore, a is close to zero. For safety, we enumerate a_0 from 0 to ± 4.5 with step increments of 0.2 or -0.2 alternately (i.e., $a_0 = 0$, 0.2, -0.2, 0.4, $-0.4, \cdots$) until solutions are found. Also, we know that $0 \leqslant b < 4.5$, so we enumerate b_0 from 0 to 4.5 with step increments of 0.5 until solutions are found. Since $0 \leqslant b + H/2 < 4.5$, H_0 is enumerated from 1 to $9 - 2b_0$ with step increments of 1 until solutions are found. Now, all the four parameters a, b, q, and H have been solved, by which we can compute curve locations to subpixel values.

Note that we do not know whether $x_1 \geqslant x_2$ or $x_1 < x_2$ before detection. There are two methods to solve this problem. One is to assume $x_1 \geqslant x_2$ first and to use (10), (11), (16), (21), and (27) to find the solution. If we cannot get a solution, try next (14)–(16), (21), and (27) to find the solution. If we cannot get a solution, try (10), (11), (16), (21′), and (27′) to find the solution. If we still cannot find a solution, finally, try (14)–(16), (21′), and (27′) to find the solution. The other method, which is used in this study, is to always assume $x_1 \geqslant x_2$ and $\bar{y}' < 0$, then use (10), (11), (16), (21), and (27) to find solutions. It is obvious that the method will fail when $\bar{y}' > 0$ or $x_1 < x_2$. In that situation, a technique is proposed to solve the problem, which will be discussed later in Section V.

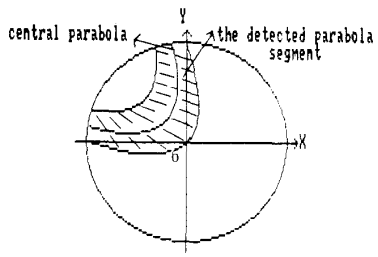

(a)

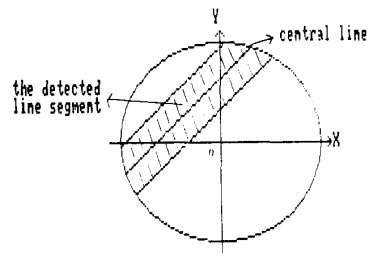

(b)

Fig. 8. Better result of proposed detector for corner finding than Chen–Tsai line detector. (a) Result of applying proposed curve detector to a)—central parabolic equation $0.324\,(0.707x + 0.707y)^2 + 1.347 = -0.707x + 0.707y$. (b) Result of applying Chen–Tsai line detector to a)—central line equation $-0.707x + 0.707y = 2.05$.

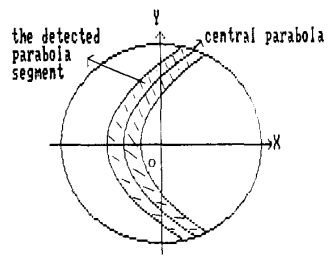

(a)

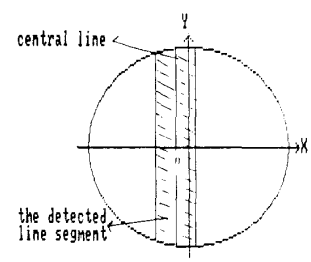

(b)

Fig. 9. Better result of proposed detector for sharp angle detection than Chen–Tsai line detector. (a) Result of applying the proposed curve detector to b)—central parabolic equation $-0.18y^2 + 1.67 = -x$. (b) Result of applying Chen–Tsai line detector to b)—central line equation $x = -0.595$.

If we set $a = 0$, it can be shown that the curve detector becomes equivalent to the Chen–Tsai line detector [14]. This means that the proposed detection can detect line features. Figs. 8, 9, 10 show the results of applying the proposed curve detector to several empirical input curve patterns. For the sake of comparison, the Chen–Tsai line detector [14] are also applied to the

same input patterns. Fig. 7 is the result of applying either the proposed curve detector or the Chen–Tsai line detector to the following two-dimensional input line pattern, which shows that the proposed curve detector has the same capability as the Chen–Tsai line detector in line detection:

```
                255 255 255 255 255
            0   0   0   0   0   0   0
        0   0   0   0   0   0   0   0   0
        0   0   0   0   0   0   0   0   0
    255 255 255 255 255 255 255 255 255
    255 255 255 255 255 255 255 255 255
    255 255 255 255 255 255 255 255 255
        255 255 255 255 255 255 255
            255 255 255 255 255.
```

Figs. 8 and 9 are the results of applying the proposed curve detector and the Chen–Tsai line detector to the following two-dimensional input curve patterns a) and b), respectively, show that the proposed detector, which is better than the Chen–Tsai line detector when a corner or a curve occurs in the detection circle:

```
a)              255   0   0 255 255
            255 255   0   0 255 255 255
        255 255 255   0   0 255 255 255 255
          0   0   0   0   0 255 255 255 255
          0   0   0   0   0 255 255 255 255
    255 255 255 255 255 255 255 255 255
    255 255 255 255 255 255 255 255 255
            255 255 255 255 255 255 255
                255 255 255 255 255;

                255 255 255   0 255
            255 255 255   0   0 255 255
        255 255 255   0   0 255 255 255 255
        255 255   0   0 255 255 255 255 255
b)  255   0   0 255 255 255 255 255 255
    255 255   0   0 255 255 255 255 255
    255 255 255   0   0 255 255 255 255
            255 255 255   0   0 255 255
                255 255 255   0 255.
```

V. The Output Format and Experimental Results

In the approach a digital image of size 256×240 is divided into a set of contiguous overlapping 4.5-unit circles as shown in Fig. 10. The distance between the centers of every two neighboring circles in the horizontal (or vertical) direction is 5 pixels.

The curve detection is repeatedly applied to each circle. A curve pattern is determined to exist in a circle if the computed h_1 and h_2 values satisfy the following inequality:

$$h_2 - h_1 \geq d. \tag{33}$$

This means that the curve pattern must be "dark" enough with respect to the background to be considered to exist in the circle. The value of d can be determined experimentally, but a more intelligent method is proposed here. By considering the original image as a blurred noisy version of a *binary* input picture, the moment-preserving bilevel thresholding proposed by Tsai [11] is applied to the whole image globally to get two representative gray levels z_0, z_1 (with $z_1 > z_0$), presumably one for the curve patterns and the other for the background. d is selected to be $(z_1 - z_0)/2$. If the original image can not be regarded as a binary version, we can divide the image into smaller nearly binary blocks and then locally apply the foregoing method to each block to get a distinct d value.

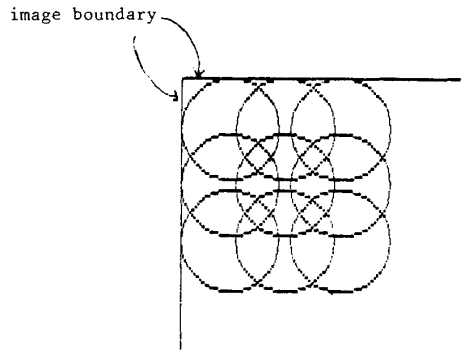

Fig. 10. Locations of detection circles used in curve detection.

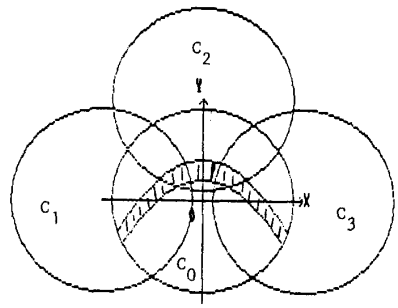

Fig. 11. Detection circle C_0 contains curve segment with $x_1 < x_2$. Neighboring detection circles C_1, C_2, and C_3 can help to detect curve segment.

In case (33) is not satisfied, we conclude that a curve pattern is not present. Otherwise, we test further for the condition:

$$\frac{h_2' - h_1'}{h_2 - h_1} \geq \delta; \tag{34}$$

where

$$h_1' = (1/a_1) \iint_{A_1} I(x, y)\, dx\, dy$$

is the mean of the observed intensities in area A_1;

$$h_2' = (1/a_2) \iint_{A_2} I(x, y)\, dx\, dy$$

is the mean of the observed intensities in area A_2; and $I(x, y)$ is the observed intensity at location (x, y) which is constant over the grid centered at (x, y). This step is employed to avoid considering as a parabolic pattern a curve that is not near a parabola or which is just noise existing in the detection circle. The threshold δ depends on the requirement for the accuracy of the detected curve. In our experiment we set δ to be 0.8. If conditions (34) as well as (33) are satisfied, then we conclude that a well-shaped parabolic pattern is present in the input circle and generate the parabolic pattern as the output. Recall that any curve pattern existing in the detection circle may have $x_1 \geq x_2$ or $x_1 < x_2$. In our implementation we always assume $x_1 \geq x_2$ and $\bar{y}' < 0$ to find a solution for any case. The reason is that when a curve segment with $\bar{y}' > 0$ or $x_1 < x_2$ exists in the detection circle, it cannot be found in the detection circle, but it may be

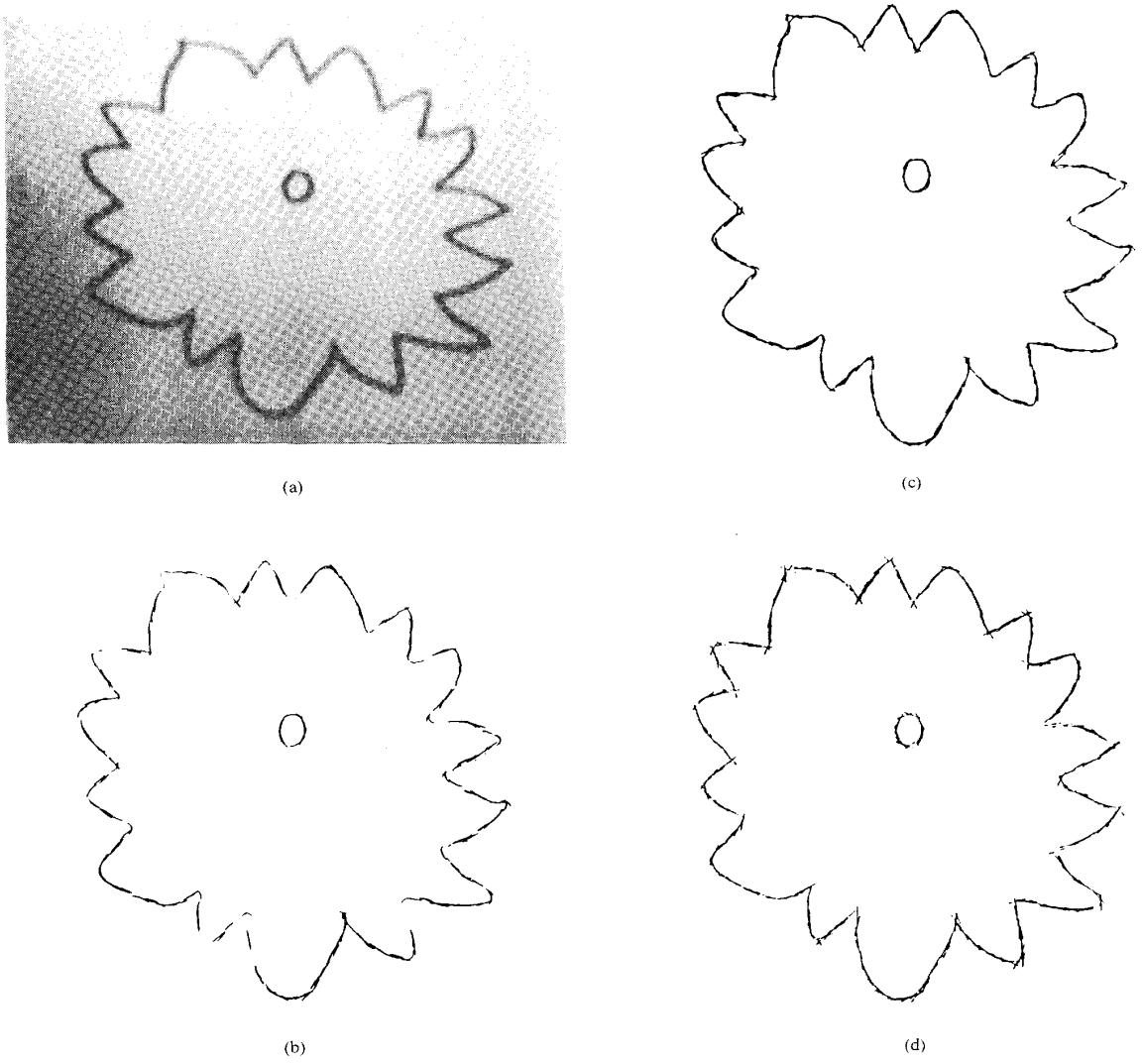

Fig. 12. Results of applying proposed curve detector and Chen–Tsai line detector to curve image. (a) Original input image. (b) Output image with 4.5-unit overlapping circles as output areas and detected central parabolas drawn in each circle area. (c) Output image resulting from detection identical to that of (b) except that curve detection is additionally applied to some of 24 neighboring points of origin (or center) of each detection circle in (b) in which curve pattern is not detected. (d) Result of Chen–Tsai line detector.

found in the neighboring detection circles (see Fig. 11 for an illustration).

Fig. 12(a) includes a drawing with many curves and sharp turns, and Fig. 13(a) includes several polygons. Figs. 12(b) and 13(b) show the results of the curve detection. In every circle of each output image, the detected central parabola is drawn according to its equation. From the output images we see that certain curve segments are missing. The reasons for this include the following: 1) the central curves of the missing curve segments are not near parabola; 2) the central parabolas do not pass through the centers of the detection circles; 3) the curve segments do not lie entirely inside the detection circles (see Fig. 14 for an illustration); or 4) $\bar{y}' > 0$ or $x_1 < x_2$. To avoid these situations, in each of such detection circles a 5×5 neighborhood of the origin is taken. Then we order the pixels in the 5×5 neighborhood by their Euclidean distances to the origin as shown:

22	15	10	14	21
16	6	2	5	13
11	3	0	1	9
17	7	4	8	20
23	18	12	19	24.

According to the order, pixels in the neighborhood are taken in turn, and the proposed curve detection procedure is applied iteratively to the 4.5-unit circle with each pixel as the center until an acceptable solution is found or until all pixels have been processed. If an acceptable curve pattern exists, then we take it as the output of the original detection circle. Note that for case $\bar{y}' > 0$ or $x_1 < x_2$ the curve segment can be detected with some of

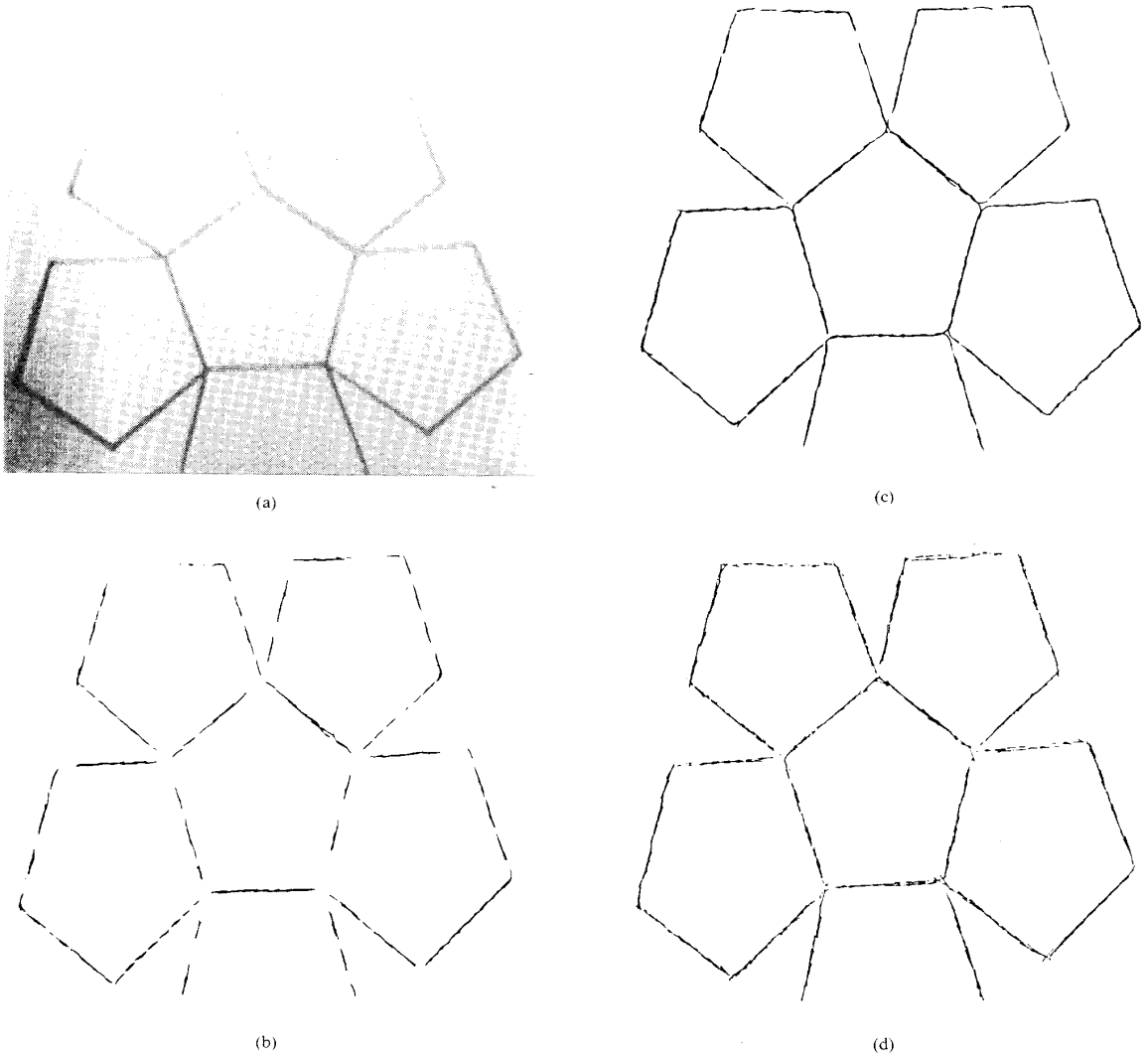

Fig. 13. Results of applying proposed curve detector and Chen–Tsai line detector to polygon image. (a) Original input image. (b) Output image with 4.5-unit overlapping circles as output areas and detected central parabolas drawn in each circle area. (c) Output image resulting from detection identical to that of (b) except that curve detection is additionally applied to some of 24 neighboring points of origin (or center) of each detection circle in (b) in which curve pattern is not detected. (d) Result of Chen–Tsai line detector.

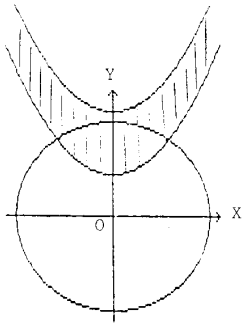

Fig. 14. Curve segment does not lie entirely inside detection circle.

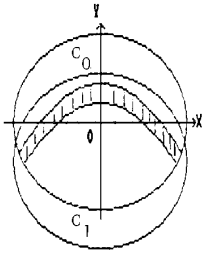

Fig. 15. Detection circle C_0 contains curve segment with $x_1 < x_2$. Some of 24 neighboring detection circles can help to detect curve segment (C_1 is example).

the 24 neighboring detection circles that have the pattern with $x_1 \geq x_2$ and $\bar{y}' < 0$ (see Fig. 15). Applying the method to Figs. 12(a) and 13(a), we have the results as shown in Figs. 12(c) and 13(c). Almost all curve segments in each image have been detected. It is seen that the proposed curve detector gives good results for curvilinear features, including lines, smooth curves, corners, and unsmooth curves. Figs. 12(d) and 13(d) show the results of line detection using the Chen–Tsai line detector. Obviously, the line detector flattens certain curve segments and does not give proper approximations at corners. The proposed curve detector on the contrary gives better results.

VI. Conclusion

If an input image includes smooth curves, lines, curves with sharp turns, and corners, almost none of the existing curve detectors can detect all of these features. They always need at least two steps to complete the detection: one for smooth curves and the other for another type of feature. In this correspondence we propose a new curve detector that can detect all these features simultaneously. Based on the moment-preserving principle and on three geometrical relations which exist in the detection circle, the approach derives a parabolic equation and a width value to approximate the curve segment. Using the derived parabolic equation, the curve location can be estimated to subpixel accuracy. The method has been tested on a variety of images and yields good results.

If a curve segment exists in the detection circle, then it separates the background into two parts. At present, the gray levels of either part are considered to be identical. It is not always true in the real world. Hence it is worth trying to remove this restriction. If a curve segment is not near a parabola, then the proposed detector is not applicable. Therefore, it is also worth trying to use curve-type equations other than the parabola to approximate curve features.

References

[1] A. Rosenfeld and A. C. Kak, *Digital Picture Processing*, vol. 2. New York: Academic, 1982.

[2] A. Rosenfeld and M. Thurston, "Edge and curve detection for visual scene analysis," *IEEE Trans. Comput.*, vol. C-20, pp. 562–569, May 1971.

[3] A. Rosenfeld, M. Thurston, and Y. H. Lee, "Edge and curve detection: further experiments," *IEEE Trans. Comput.*, vol. C-21, pp. 677–715, July 1972.

[4] Z. Q. Wu and A. Rosenfeld, "Filtered projections as an aid in corner detection," *Pattern Recognition*, vol. 16, no. 1, pp. 31–38, 1983.

[5] K. Paler, J. Foglein, J. Illingworth, and J. Kittler, "Local ordered grey levels as an aid to corner detection," *Pattern Recognition*, vol. 17, no. 5, pp. 535–543, 1984.

[6] P. V. C. Hough, "Method and means for recognizing complex patterns," US Patent 3069654, 1962.

[7] R. O. Duda and P. E. Hart, "Use of the Hough transformation to detect lines and curves in pictures," *Commun. Ass. Comput. Mach.*, vol. 15, no. 1, pp. 11–15, 1972.

[8] S. D. Shapiro, "Generalization of the Hough transform for curve detection in noisy digital images," in *Proc. 4th Int. Joint Conf. Pattern Recognition*, Kyoto, Japan, Nov. 1978, pp. 710–714.

[9] D. H. Ballard, "Generalizing the Hough transform to detect arbitrary shapes," *Pattern Recognition*, vol. 13, no. 2, pp. 111–122, 1981.

[10] A. J. Tabatabai and O. R. Mitchell, "Edge location to subpixel values in digital imagery," *IEEE Trans. Pattern Anal. Mach. Intell.*, vol. PAMI-6, pp. 188–201, 1984.

[11] W. H. Tsai, "Moment-preserving thresholding: A new approach," *Comput. Vision, Graphics, Image Process.*, vol. 29, pp. 377–393, 1985.

[12] L. H. Chen and W. H. Tsai, "Moment-preserving sharpening: A new approach to digital picture deblurring," *Comput. Vision, Graphics, Image Process.*, to be published.

[13] ____, "Location of curved edges to subpixel values," to be published.

[14] ____, "Moment-preserving line detection," *Pattern Recognition*, to be published.

[15] J. L. Synge and B. A. Griffith, *Principles of Mechanics*. New York: McGraw-Hill, 1949, pp. 75–76.

[16] C. F. Gerald and P. O. Wheatley, *Applied Numerical Analysis*. Reading, MA: Addison-Wesley, 1983, p. 135.

Convolution Operators as a Basis for Objective Correlates of Texture Perception

K. K. BENKE, D. R. SKINNER, AND C. J. WOODRUFF

***Abstract*—A method is described for deriving, from digitized images, objective measures that correlate strongly with simple perceptual judgements on the same images. Each measure is the normalized variance of an image obtained by convolving the original image with a specific local operator. This operator is designed to optimize the correlation between the particular percept and the objective measure, subject to certain constraints.**

I. Textural Features

The analysis and characterization of visual textures is an important requirement for both human and machine vision. Mathematical approaches have been developed for the purposes of feature extraction, pattern recognition, and scene segmentation, as summarized in the surveys of Haralick [1] and Van Gool *et al.* [2]. Machine discrimination of textures is an area of considerable interest, requiring measurement of specific features rather than a knowledge of the underlying structure and synthesis of the texture. It would be of value if measures on digital images of textures could be found that correlated with human performance in discriminating these textures.

In a significant experiment, Tamura *et al.* [3] attempted to relate objective measures of digitized textures to psychophysical judgements of the same textures on the basis of defined perceptual criteria. They implemented different computational procedures for each of six scales, and obtained rank correlations in the range 0.65 to 0.90 between the psychological and objective measures. In this paper, we investigate further the problem of finding measures on the digitized image that correlate highly with human perception of texture.

The results from our experiments suggest that the optimization of a local operator offers the prospect of a general technique for the determination of objective measures. There is an important difference between our approach and that of Tamura *et al.* They aimed at measuring the correspondence between computational definitions of textural features and psychophysical assessments. We have decided to use a general operator and adjust its parameters so as to optimize the correlation between objective measures and psychophysical assessments. The psychological assessment of the textures used by Tamura *et al.* required a judgement based on a verbally defined textural feature.

We investigated three perceptual scales similar to those used in [3]. Subjects were asked to separately allocate images of textures along each of three psychological scales. These were line-like versus bloblike nondirectional versus directional (where monodirectionality was ranked above bidirectionality), and random versus regular.

II. Objective Measures of Textural Features

In developing a mathematical approach to the problem of texture characterization, we will describe the texture in statistical rather than structural terms [1], [2]. The texture field is analysed by computing the statistics of the local properties after filtering with a convolution mask [4], [5]. In the past, these operators have inspired models for edge detection because of their similarities to the feature extractors believed to exist in the human visual system, as described, for example, by Marr [6].

Manuscript received Feb. 21, 1987; revised Nov. 3, 1987.

The authors are with the Australian Department of Defence, Materials Research Laboratories, P.O. Box 50, Ascot Vale, Victoria 3032, Australia.

IEEE Log Number 8718873.